

Nanoindentation of polydimethylsiloxane elastomers: Effect of crosslinking, work of adhesion, and fluid environment on elastic modulus

Fernando Carrillo

Department of Orthopaedic Surgery, University of California—San Francisco, San Francisco, California 94110; and Department of Chemical Engineering, EUETIT – Polytechnic University of Catalonia, Terrassa E-08222, Spain

Shikha Gupta

Medical Polymers Group, Department of Applied Science and Technology, University of California—Berkeley, Berkeley, California 94720

Mehdi Balooch

Department of Preventive and Restorative Dental Sciences, University of California—San Francisco, San Francisco, California 94143

Sally J. Marshall and Grayson W. Marshall

Department of Preventive and Restorative Dental Sciences, University of California—San Francisco, San Francisco, California 94143; and University of California—Berkeley/University of California—San Francisco, Bioengineering Joint Graduate Group, San Francisco, California 94143

Lisa Pruitt

Department of Mechanical Engineering, University of California—Berkeley, Berkeley, California 94720; and University of California—Berkeley/University of California—San Francisco, Bioengineering Joint Graduate Group, San Francisco, California 94143

Christian M. Puttlitz^{a)}

Department of Orthopaedic Surgery, University of California—San Francisco, San Francisco, California 94110, and University of California—Berkeley/University of California—San Francisco, Bioengineering Joint Graduate Group, San Francisco, California 94143

(Received 14 December 2004; accepted 14 July 2005)

With the potential to map mechanical properties of heterogeneous materials on a micrometer scale, there is growing interest in nanoindentation as a materials characterization technique. However, nanoindentation has been developed primarily for characterization of hard, elasto-plastic materials, and the technique has not been validated for very soft materials with moduli less than 5 MPa. The current study attempted to use nanoindentation to characterize the elastic moduli of soft, elastomeric polydimethylsiloxane (PDMS) samples (with different degrees of crosslinking) and determine the effects of adhesion on these measurements using adhesion contact mechanics models. Results indicate that nanoindentation was able to differentiate between elastic moduli on the order of hundreds of kilo-Pascals. Moreover, calculations using the classical Hertz contact model for dry and aqueous environment gave higher elastic modulus values when compared to those obtained from unconfined compression testing. These data seem to suggest that consideration of the adhesion energy at the tip-sample interface is a significantly important parameter and needs to be taken into account for consistent elastic modulus determination of soft materials by nanoindentation.

I. INTRODUCTION

For bulk materials, mechanical properties like hardness and elastic modulus are readily described using standard characterization methods such as compression

and tensile tests. Determination of the mechanical properties of soft and anisotropic materials, such as biological tissues, is complicated by the heterogeneous nature of the tissue, so that the aforementioned bulk testing methods may not be applicable due to inadequate sample dimensions.¹ Thus, techniques that allow for the examination of the mechanical properties at the microstructural level are clearly needed in many basic sciences and applied bioengineering applications.

^{a)}Address all correspondence to this author.

e-mail: puttlitz@engr.colostate.edu

DOI: 10.1557/JMR.2005.0354

Nanoindentation is a technique that has recently received a great deal of attention and provides a method for determining material properties on a much reduced scale. Specifically, this technique may be applicable for studying the mechanical response of biological materials on the micrometer or nanometer scale. Direct physical property measurement of heterogeneous biological materials, such as friction, adhesion, and elasticity, can be determined with high spatial resolution. In addition, the time-dependent mechanical properties of these materials can be obtained in aqueous (saline) environments, providing a means for property determination that approximates the in situ tissue environment.

The nanoindentation technique has traditionally been used to characterize the elasto-plastic properties of hard materials, most commonly by the analysis of Oliver and Pharr.^{2,3} This method determines elastic moduli from the unloading portion of the indentation load-displacement behavior. Many groups have used this methodology to measure the material properties of hard, mineralized biological tissues.^{4–11} Moreover, there have been some preliminary studies on soft tissues, such as demineralized dentin,^{12,13} cartilage, and vascular tissues.^{14,15} However, the Oliver–Pharr load-displacement analysis is based upon elastic contact theory, and the applicability of this method to describe materials that exhibit significant viscoelastic behavior has not been extensively explored.¹⁶ In addition, the aforementioned elastic contact analysis does not account for the possibility of adhesion forces. For example, the experimental load-displacement data gives an indirect measure of the contact area, from which the elastic modulus is calculated. Therefore, the relationship between the contact area and the load is important and factors that affect this relationship need to be identified and incorporated into an appropriate material model. In particular, the influence of interfacial adhesive forces on nanoscale deformation, which can affect the indentation contact area, should be considered for accurate nanoindentation material property characterization and modeling.^{17,18}

Nanoindentation has not been validated for measuring mechanical properties of very soft materials (elastic modulus below 5 MPa). Given the sophistication of currently available analytical techniques, the application and validation of using nanoindentation techniques to obtain accurate soft tissue material properties could have a profound impact on the ability to simulate, via computational analyses, the mechanical environment of numerous biological systems. Thus, the goal of the current study was to determine if nanoindentation could be used to measure the mechanical properties of soft materials. Particularly, this study explores the application of using the nanoindentation technique to characterize the elastic modulus (E_s) of elastomeric polydimethylsiloxane (PDMS) as a function of the different degrees of

crosslinking. In addition, the effect of the work of adhesion on these measurements using adhesion contact mechanics models is also presented. Finally, the effect of the indentation environment (dry versus aqueous) on the resultant elastic modulus determination was elucidated.

II. MATERIALS AND METHODS

The overall study design focuses on the elastic moduli determination of a series of elastomeric PDMS samples of various concentrations. These mechanical properties were obtained using nanoindentation and a more conventional technique, unconfined compression, and the data were compared to determine the degree of precision offered by the nanoindentation method. Although PDMS is technically classified as a viscoelastic elastomer ($\tan \delta < 0.01$),¹⁹ at room temperature it has been shown that PDMS can be considered to be nearly incompressible (Poisson's ratio ≈ 0.5)²⁰ and its mechanical behavior can be approximated by classical linear elasticity.^{21–24} Thus, these simplifications were incorporated in the current analysis.

A. PDMS sample preparation

PDMS elastomer samples were prepared by mixing different ratios of a siloxane base with a cross-linker agent (Sylgard Elastomer 184, Dow Corning Corporation, Midland, MI). Five ratios of base to cross-linker agent were used (10:1, 15:1, 20:1, 25:1, and 30:1), with higher ratios resulting in a softer, less cross-linked elastomer. Three specimens of each ratio were prepared for a total of 15 samples. Each solution was stirred for 10 min at room temperature, and 2.5 g of each concentration was subsequently poured into a 10-mm-diameter plastic container with a microscope glass slide providing the bottom surface boundary. Use of the glass slide facilitated obtaining a smooth surface for indentation. All samples were then covered with a lid and cured at room temperature for 2 weeks. After curing, $5 \times 5 \times 2.5$ mm samples were cut from the bulk elastomer and glued to a metal platen. Sample surfaces were kept covered with a microscope slide prior to testing to avoid contamination. The mechanical properties of all samples were then determined via nanoindentation and unconfined compression experiments.

B. Surface roughness evaluation

To assess the surface roughness of the various samples, $20 \mu \times 20 \mu\text{m}$ topographical images of the PDMS samples were obtained by atomic force microscopy (AFM; Nanoscope IIIa, Multimode, Picoforce force control module, DI-Veeco Instruments Inc., Santa Barbara, CA) in TappingMode. The tapping-mode imaging conditions included a 1 Hz scan rate, 512 points collected

per line (pixel resolution), and a 1.0 V set point. Surface probing was performed using a silicon tip (Nanosensors, Germany) with a nominal spring constant in the range of 27–47 N/m, a length of 123 μm, and a nominal radius of curvature less than 10 nm. The microtopography and the arithmetic mean surface roughness (R_a , nm) of the scanned areas were calculated using bundled software (Nanoscope III version 6.12r1, Nanoscope, Multimode, DI-Veeco Instruments Inc.) using the following equation²⁵

$$R_a = \frac{1}{N} \sum_{i=1}^N |Z_i - Z_m| \quad , \quad (1)$$

where N is the number of points within a given area, Z_i is the current height (z-scale) of the i th point, and Z_m is the z value of the center plane (mean surface height).

C. Unconfined compression

Bulk unconfined compression tests were conducted on a standard tension/compression materials testing system (EnduraTec, Bose Electroforce 3200, Minnetonka, MN) with 0.1 N and 0.01 mm load and displacement resolutions, respectively. A final displacement of 0.25 mm, or approximately 10% strain, was applied to each sample using a displacement rate of 0.25 mm/s. The quasi-static elastic modulus was calculated assuming linear elastic constitutive behavior of the PDMS samples

$$E_s = \frac{\sigma_s}{\epsilon} \quad , \quad (2)$$

where σ_s and ϵ are the engineering stress and strain, respectively.

D. AFM based nanoindentation

1. Contact mechanics models

a. Hertz linear elastic analysis

Based on classical Hertzian contact theory,^{26,27} the load (P) applied to the indenter tip is related to the total penetration depth into the substrate (h). Due to the spherical geometry of the indenter tip, this deformation is directly related to the contact radius (a) using the following relationship

$$a^3 = \frac{6R}{8E_r} P \quad , \quad (3)$$

where E_r is the reduced elastic modulus and R is the nominal radius of curvature of the conospherical tip. The reduced modulus E_r is related to the elastic modulus of the substrate as²⁷

$$\frac{1}{E_r} = \left[\left(\frac{1 - \nu_s^2}{E_s} \right) + \left(\frac{1 - \nu_i^2}{E_i} \right) \right] \quad , \quad (4)$$

where E is the steady state elastic modulus and ν the Poisson's ratios of the substrate (subscript s) and the indenter (subscript i). In the current investigation, the elastic modulus of the indenter tip is many orders of magnitude higher than the elastic modulus of substrate (rigid body indenter condition). Accordingly, the second term in Eq. (4) was neglected. From Hertz elastic analysis, the stiffness (S) is related to the contact radius (a)

$$S = \frac{dP}{dh} = 2aE_r \quad . \quad (5)$$

Combining the previous equations [Eqs. (3–5)] leads to the following expression for the elastic modulus for spherical indentation

$$E_s^{\text{Hertz}} = \sqrt{\frac{S^3(1 - \nu_s^2)^2}{6RP}} \quad . \quad (6)$$

b. Oliver and Pharr analysis

More recently, Oliver and Pharr² derived expressions for calculating the elastic modulus from indentation experiments based on Sneddon's²⁸ elastic contact theory

$$E_r = \frac{S\sqrt{\pi}}{2\beta\sqrt{A_c}} \quad , \quad (7)$$

where S is the unloading stiffness and is taken to be the initial slope of the unloading load-displacement curve at the maximum depth of penetration (or peak load), A_c is the projected contact area between the tip and the substrate at peak load and β is a constant that depends on the geometry of the indenter ($\beta = 1$ for circular contact). For circular contact, the contact area can be calculated using the ideal geometric area function

$$A_c = \pi(2Rh_c - h_c^2) \quad , \quad (8)$$

where h_c is the contact depth at peak load which is estimated by

$$h_c = h_m - \epsilon \frac{P_m}{S_m} \quad , \quad (9)$$

where h_m is the total penetration depth of the indenter at peak load, P_m is the peak load at the indenter displacement depth h_m , and ϵ is an indenter geometry constant, equal to 0.75 for spherical indenters.

In the absence of adhesion, the elastic modulus was calculated using both the Hertz [Eq. (6)] and Oliver and Pharr [Eq. (7)] formulations based on stiffness measurements taken from the unloading data of the experimental load-displacement curves.

2. Nanoindentation measurements

Nanoindentation measurements were performed using a Hysitron TriboIndenter (Hysitron Inc., Minneapolis, MN) in a load-controlled instrument with load and displacement resolutions of 100 nN and 1 nm, respectively. The system is capable of attaining a maximum indentation depth of approximately 5 μm . A 100- μm radius of curvature conospherical diamond probe tip was used as an indenter (Fig. 1).

Quasi static indentation testing was performed at room temperature using a trapezoidal load versus time profile with a loading and unloading rate of 10 $\mu\text{N/s}$, a peak load of 100 μN , and a hold period of 10 s (30 s total time profile). After the indenter tip made contact with the specimen surface, the aforementioned preload was applied, and the indentation load and depth were recorded simultaneously. The low stiffness of the PDMS samples as well as the stiffness of the tip assembly (system compliance) resulted in relatively large tip displacements. Similarly, the combined compliance of the measurement system and sample contributed to the overall mechanical behavior. Thus, for a given input voltage, the load applied to the sample varied depending on the sample stiffness. However, the actual load magnitude applied to the sample was measured independently, and all subsequent calculations were based upon these accurate force measurements. This effect significantly influenced the forces detected by the system, leading to load values which were less than the nominal 100 μN peak load that was applied (approximately 20 to 8 μN for stiff and soft samples, respectively). Pilot experiments demonstrated that there was not significant drift during the 30 s indentation time course. Specifically, after force equilibrium, using least squares linear fit, the rate of drift was found to be within 0.01–0.02 nm/s. This is translated into a maximum indenter drift within 0.3–0.6 nm for a test that lasts 30 s. Accordingly, system drift rate was neglected. Eight indents were performed in different places on each

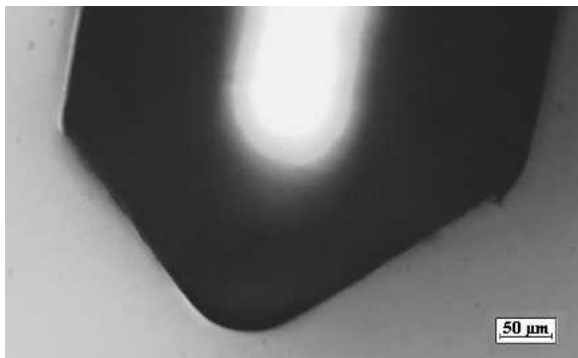


FIG. 1. Optical microscopy image of the conospherical diamond probe tip of 100 μm radius of curvature used as indenter.

sample at room temperature (24 $^{\circ}\text{C}$) under both dry (relative humidity of 54%) and aqueous conditions. Specifically, the sample was completely submerged in distilled water, and the indentation experiment occurred such that the contact occurred completely in the aqueous solution. Experiments in water were conducted for one randomly selected sample of each concentration. From the load-displacement nanoindentation data, the elastic modulus of the substrate (E_s) was calculated using elastic continuum contact mechanics models [Eqs. (6), (7), (12)].

E. Adhesion modeling and measurements

1. Adhesion contact mechanics models

The classical Hertzian model is representative of hard contact between two spherical elastic bodies. This model is valid if the interfacial adhesive forces are much lower than the applied compressive force between the indenter and substrate. The presence of interfacial forces increases the effective contact area predicted by the Hertzian solution and several continuum mechanics models have been proposed to include this adhesive effect.^{17,29–34} The load dependence of the contact area is affected by the strength of the adhesive forces as compared to the elastic deformations

$$a^3 = \frac{6R}{8E_r} f(P, F_{po}) \quad , \quad (10)$$

where f is a function of the load (P) and the maximum adhesive pull-off force (F_{po}) between the tip and the sample. The two most common models used to describe the effect of adhesion on contact mechanics behavior are the Johnson, Kendall, Roberts (JKR)²⁹ and Derjaguin–Muller–Toporov (DMT) models.³⁰ Physically, the JKR theory accounts for adhesion forces only within the expanded area of contact. The JKR model should be used for low modulus materials with high surface energy and large radius of curvature. On the other hand, the DMT theory accounts for adhesion forces outside the contact area while maintaining the Hertzian gap profile. The DMT model is most applicable to high modulus materials with low surface energy and small radius of curvature. Thus, the JKR model is more appropriate for our experimental conditions. In fact, it has been successfully applied to previous PDMS indentation studies.³⁵ According to the JKR model, the work of adhesion is related to the magnitude of the maximum tensile pull-off adhesion force introduced in Eq. (10)

$$F_{po}^{JKR} = \frac{3}{2} \pi R W_A \quad , \quad (11)$$

where W_A is the thermodynamic work of adhesion per unit of contact area. According to Johnson,²⁷ W_A is the work required to separate two surfaces (such as the tip

and substrate) from contact to infinite separation. Inclusion of the adhesion force in Eq. (11) to the Hertzian contact equation [Eq. (6)] leads to the JKR expressions for the elastic modulus for spherical indentation

$$E_s^{JKR} = \sqrt{\frac{S^3(1-\nu_s^2)^2}{6R} \left[\frac{1}{P + 2F_{po}^{JKR} + 2F_{po}^{JKR} \sqrt{\left(\frac{P}{F_{po}^{JKR}} + 1\right)}} \right]} \quad (12)$$

2. Adhesion measurements

To assess the contribution of interfacial adhesive forces, as described by Eq. (12), the pull-off force F_{po} was experimentally determined prior to each individual indentation using AFM, to which a load-displacement transducer (Triboscope Micromechanical Test Instrument, Hysitron Inc.) was attached. This equipment provided load and displacement resolutions of 1 μ N and 1 nm, respectively. The principle of this experiment was to put into contact the diamond conospherical probe tip and the flat polymer substrate and determine the maximum force (F_{po}) necessary to separate both materials. In each test the conospherical tip (100 μ m radius of curvature diamond probe tip) was brought into contact with the sample surface using a displacement rate of 1 μ m/s. After applying an initial preload of 20 μ N, a profile of the transducer force and displacement versus time was collected while the sample was retracted at 100 nm step intervals using the AFM motor control. If interfacial forces were present, the transducer force became negative and the tip plate continued to move with the sample until the negative restoring force on the transducer became equal to the adhesive force between the tip and PDMS surface interface. The pull-off adhesion force F_{po} was determined as the difference between the minimum force value and the zero offset. Five adhesion tests on surface regions of each sample were performed for each PDMS concentration in dry and aqueous conditions to study the effect of fluid environment on adhesion.

F. Statistical analysis

To delineate specific differences in elastic moduli and adhesion forces between different PDMS concentrations obtained from both unconfined compression and nanoindentation experiments, statistical analyses were performed using a one-way analysis of variance (ANOVA) with Fisher's least-significant-difference PLSD post hoc test for multiple comparisons (Statview for Windows, version 5.0, SAS Institute Inc., NC). In all cases, p-values smaller than 0.05 were considered statistically significant.

III. RESULTS AND DISCUSSION

A. Surface roughness

AFM topography scans of different PDMS specimens were used to determine their surface roughness by the calculation of the arithmetic mean surface roughness R_a (Fig. 2). AFM images showed an R_a average of 6.6 ± 2.1 nm across all PDMS substrates. This data confirmed that the samples were significantly packed at the submicrometer level and that the sample preparation method produced relatively smooth surfaces for indentation. This data demonstrated that surface roughness should not be considered a confounding factor on the nanoindentation and adhesion results.

B. Unconfined compression test

Values of elastic moduli were obtained from unconfined compression experiments (shown with the nanoindentation results in Fig. 7). As expected, the more cross-linked structures had higher elastic moduli. The mean elastic moduli of the PDMS samples ranged from 2.04 ± 0.06 MPa (10:1 mixture, mean \pm standard deviation) to 0.42 ± 0.05 MPa (30:1 mixture). Each increase in ratio of base to cross-linking agent produced a significant ($p < 0.05$) reduction in the compressive elastic modulus.

C. Adhesion

Interfacial adhesive pull-off forces were determined for each specimen using the AFM nanoindentation instrument. Typical unloading curves obtained during the

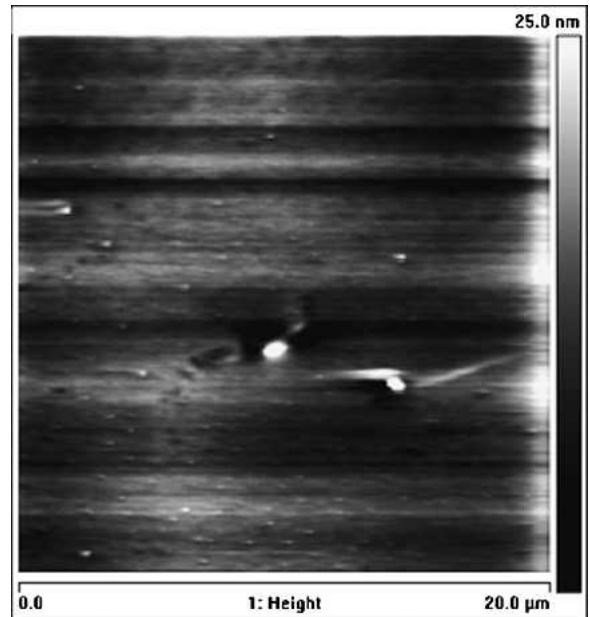


FIG. 2. Typical topographic $20 \times 20 \mu$ m AFM image (TappingMode) of a PDMS sample (10:1 concentration, $R_a = 8.3$ nm). The z-scale is 0 (dark) to 25 nm (light). The mean surface roughness (R_a) was 6.6 ± 2.1 nm across all PDMS samples.

adhesion experiments in dry conditions are shown in Fig. 3. Pilot experiments were conducted at different initial contact preloads to study its influence, if any, on the adhesion pull-off force measurements (Fig. 4). This data demonstrates that the initial contact preload (5–50 μN) has a minor influence on the pull-off force and that this independence was most prominent for the stiffer PDMS samples. Only the most compliant PDMS samples demonstrated a decrease of the adhesion work at initial preload values higher than 20 μN . To avoid working in this range of initial preload dependence that may confound the subsequent experiments, and considering the fact that the maximum force applied to the samples during nanoindentation measurements was 20 μN (corresponding to the stiffer PDMS), an initial preload force of 20 μN was selected for the adhesion testing of all PDMS samples in dry and aqueous conditions. Due to system limitations, use of a constant unloading value was not possible; however, the unloading rate varied in a small range (1500–1900 $\mu\text{N/s}$). Within this unloading range no significant influence of the unloading rate on the pull-off force was detected (Fig. 3), although a thorough investigation at several different unloading rates was not conducted to fully determine the effect of rate on the adhesion behavior.

The adhesion pull-off force (F_{po}) was determined for each sample. No significant differences ($p < 0.0001$) were found between the three different samples of each concentration, indicating reproducibility of the sample preparation method. The mean adhesion pull-off force data measured in dry conditions is shown in Fig. 5 (shown with the aqueous pull-off force results). The adhesion pull-off forces of PDMS ranged from $93.1 \pm 6.8 \mu\text{N}$ (for 10:1 concentration) to $43.6 \pm 3.6 \mu\text{N}$ (for 30:1 concentration). In general, the more compliant samples tended to exhibit lower pull-off forces. There

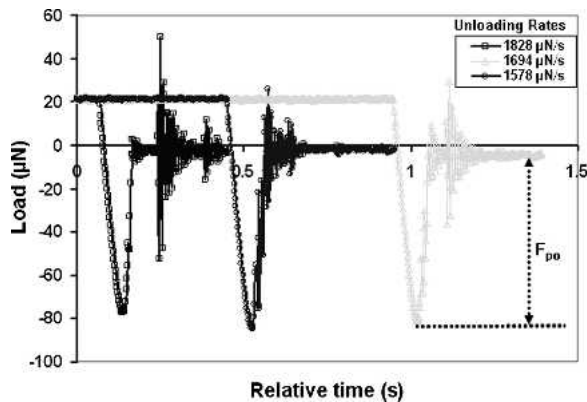


FIG. 3. Typical pull-off force behavior obtained from an AFM adhesion experiment on PDMS 15:1 substrate (dry conditions) for different unloading rates using a conospherical diamond tip of 100 μm radius of curvature. No significant influence of the unloading rate (1500–1900 $\mu\text{N/s}$) on the pull-off force was observed.

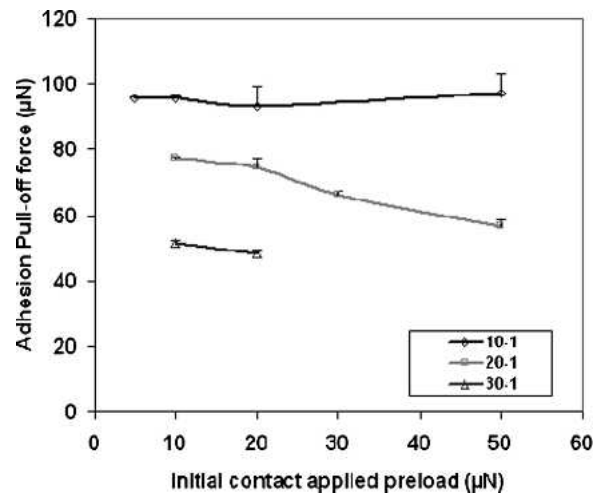


FIG. 4. Influence of the initial contact preload on the adhesion pull-off force determined in dry conditions (mean with one standard deviation error bars). Note significant preload dependence for compliant PDMS samples at preload values higher than 20 μN .

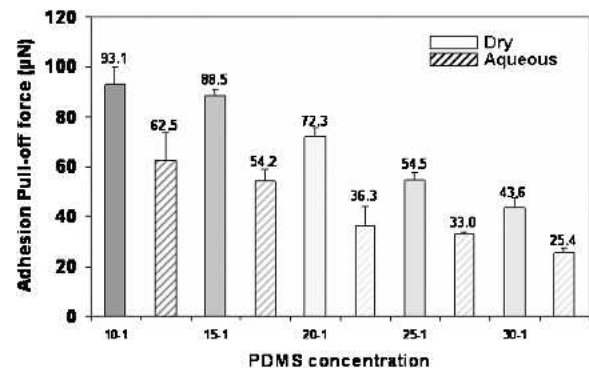


FIG. 5. Adhesion pull-off force of each group of PDMS substrates measured in dry and aqueous conditions (mean with one standard deviation error bars). Significant decreases ($p < 0.001$) in F_{po} with decreasing cross-linking (soft samples) was observed in dry conditions for all the PDMS concentrations. Significant decrease in the adhesion force was obtained in aqueous conditions for all PDMS concentrations.

were significant differences ($p < 0.021$) in adhesion pull-off forces between each PDMS concentration. It clearly appears (Fig. 5) that the F_{po} is continuously lower for soft materials (less cross-linking). This behavior can be mainly attributed to differences in the degree of cross-linking (lower cross-linking density induces higher chain length between chemical nodes for soft samples) between the samples that influence the number and energy of the interactions involved, and ultimately, determines the gestalt interfacial properties between the tip and each PDMS substrate.^{18,36–38}

Adhesion experiments were also conducted in an aqueous solution to study the influence of experimental environment on the adhesion work (Fig. 5). The results indicate a significant decrease ($p < 0.001$) in the adhesive force when testing was performed in distilled water for

each concentration. Since the contribution of electrostatic attraction to the total adhesive force is relatively large for PDMS³⁸ (in addition to the dispersive interactions due to the non-polar behavior of PDMS), the decrease in the measured F_{po} is probably the result of the weakening of the electrostatic charge under wet conditions. Moreover, the F_{po} values do not seem to be converging to zero. This is most probably due to the repellant interaction of PDMS (an inherent hydrophobic material mainly due to the presence of $-CH_3$ groups) with water, and the constant presence of these dispersive van der Waals forces. In addition, aqueous measurements show a continuously lower F_{po} value for compliant samples. This trend agrees with the general behavior obtained for the dry experiments. There were significant differences ($p < 0.001$) in adhesion pull-off forces measured in distilled water between the stiffest samples (10:1 and 15:1 concentrations) and the softest samples (20:1, 25:1, and 30:1 concentrations). Aqueous measurements did not show a significant difference in F_{po} between the softer PDMS concentrations, indicating a similar surface energy and apparently similar contact interactions of these PDMS samples. Overall, the results show that the adhesion forces between the tip and PDMS substrates are not negligible, and should be taken into account.

D. Nanoindentation

1. Nanoindentation in dry environment

Nanoindentation experiments were performed on the five PDMS concentrations ($n = 3/\text{concentration}$). The typical indentation curves obtained in dry conditions for a representative sample of each PDMS concentration are shown Fig. 6. Similar trends in mechanical behavior are exhibited by all the samples. Specifically, lower loads and deeper indentation depths were achieved with less cross-linked samples (higher base to cross-linker ratio). In addition, no significant variability was found among

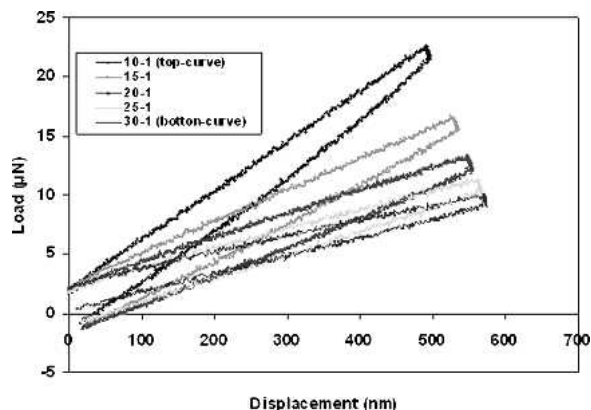


FIG. 6. Typical nanoindentation load-displacement curves for each PDMS concentration (dry conditions).

indentations of different samples of each PDMS concentration, indicating reproducibility of the sample preparation and testing method. Thus, the data were pooled with the mean and the standard deviation calculated for all the samples of the same concentration.

Taking into account the previously determined adhesion pull-off force, the elastic moduli of the samples were calculated for the previously presented adhesion model [Eq. (12)]. Elastic moduli were also determined using the classical Hertzian contact model [Eq. (6)] and the standard Oliver and Pharr unloading stiffness analysis [Eq. (7)], assuming incompressible ($\nu_s = 0.5$) linear elastic behavior of the samples.

The mean elastic moduli results obtained via nanoindentation in dry conditions using the Oliver and Pharr, Hertzian, and JKR models are shown in Fig. 7. These data are compared with the elastic moduli obtained from the aforementioned unconfined compression experiments. There were significant differences ($p < 0.03$) between the elastic moduli calculated for each PDMS concentration, regardless of the model used. The results demonstrate that nanoindentation is capable of differentiating between elastic moduli of soft materials with values on the order of hundreds of kilo-Pascals.

Using the PDMS elastic moduli obtained from unconfined compression testing as the reference data, calculations using the Oliver and Pharr analysis and the Hertzian model resulted in higher modulus values. The elastic moduli obtained via the Oliver and Pharr method gave significantly higher values ($p < 0.001$) than the data obtained from performing a classical Hertzian contact analysis. This difference appears due to the assumption in the Hertz formulation that the contact depth (h_c) is related to the total penetration depth (h) by $h = 2h_c$. In the Oliver and Pharr analysis, the contact depth (h_c) is estimated using Eq. (9). Only for ideal elastic contact ($h = 2h_c$) will both analysis compute the same moduli. Our experimental results from these two models dictate that $h = (2.8 \pm 0.3)h_c$ in order for these models to be equivalent. These data indicate that there is a deviation from the elastic contact assumption inherent in these two models and explains the different elastic moduli obtained from each analysis.

2. Nanoindentation in aqueous environment

Nanoindentation measurements were also conducted in distilled water, for one sample of each PDMS concentration, to study the influence of experimental fluid environment on the elastic moduli. Figure 8 shows the elastic moduli calculated using the Oliver and Pharr analysis using data obtained in both dry and aqueous environments. The data indicate a significant decrease ($p < 0.001$) in the elastic modulus when testing was performed in an aqueous environment for each PDMS concentration. The same behavior is shown comparing the

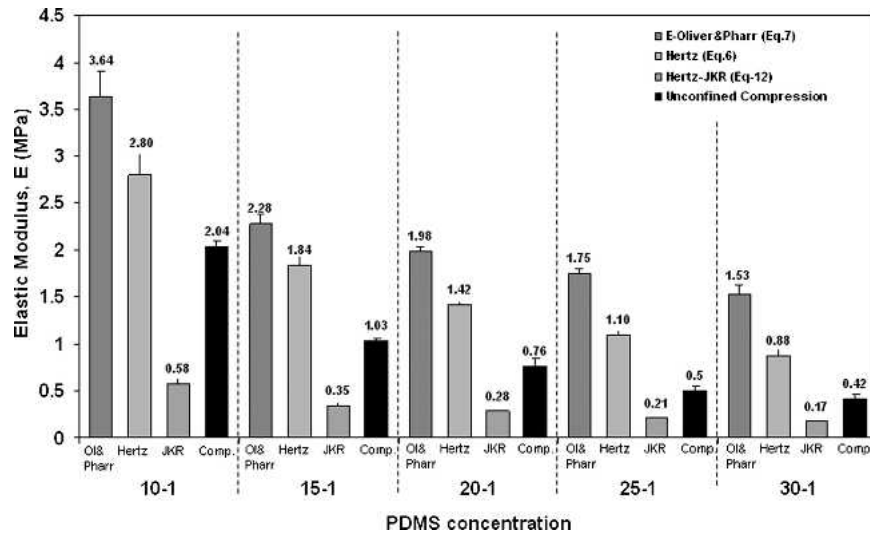


FIG. 7. Elastic moduli obtained from the nanoindentation experiments (dry conditions) using the Oliver and Pharr, Hertz, and JKR models (left to right). For comparison, the unconfined compression elastic moduli results are also shown for each PDMS concentration. Significant differences ($p < 0.03$) between the elastic moduli calculated for each PDMS concentration were observed, regardless of the model used.

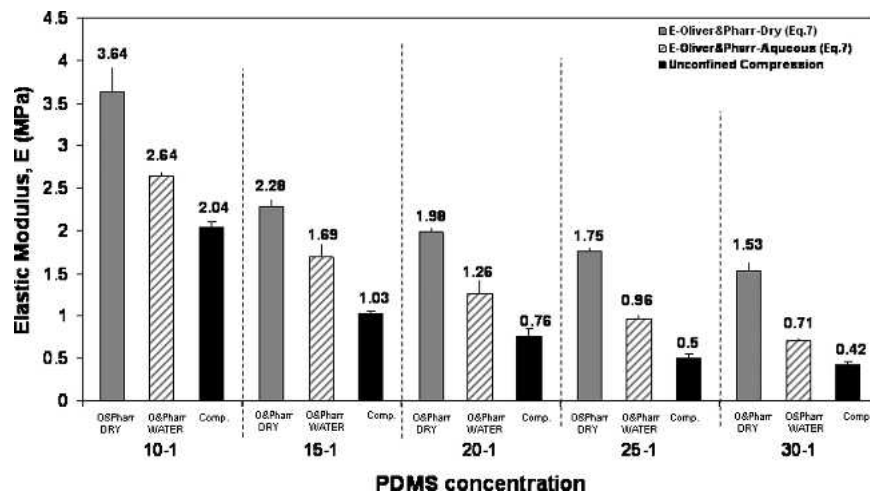


FIG. 8. Comparison of elastic moduli obtained from the nanoindentation experiments in dry and aqueous environments using the Oliver and Pharr analysis. For comparison, the unconfined compression elastic moduli are also shown for each PDMS concentration. A significant decrease ($p < 0.01$) in the elastic moduli was observed in the aqueous environment (as compared to dry conditions) for all PDMS concentrations.

results obtained using Hertz analysis (Figs. 7 and 9 for Hertz results in dry and aqueous, respectively). As discussed previously, a decrease in the adhesion pull-off force was observed when using the same aqueous environment mainly due to the weakening of the electrostatic charges. Thus, the decrease in the observed interfacial adhesion force when testing in distilled water could explain this decrease in elastic moduli. Accordingly, high elastic modulus values are estimated when using non-adhesion contact models.

In addition, no significant ($p > 0.05$) differences between the calculated elastic moduli from classical Hertz and Oliver and Pharr analyses were found in the aqueous measurements as compared to the results obtained in dry conditions (Fig. 9). The new relationship between the

contact depth and total penetration in the aqueous environment measurements was $h = (2.4 \pm 0.5)h_c$. Although this represents a deviation from ideally elastic contact ($h = 2h_c$), the relation obtained in fluid is closer to the ideal behavior than the relationship obtained for dry measurements. Moreover, if the contribution from adhesion force is considered, no significant differences ($p > 0.05$) between the elastic moduli results obtained using JKR in dry and wet conditions were found (Figs. 7 and 9). These results indicate that adhesive forces must be considered to obtain consistent elastic moduli of the PDMS samples.

Application of the JKR adhesion contact model [Eq. (12)] estimates elastic moduli values which were significantly lower ($p < 0.013$) than the expected

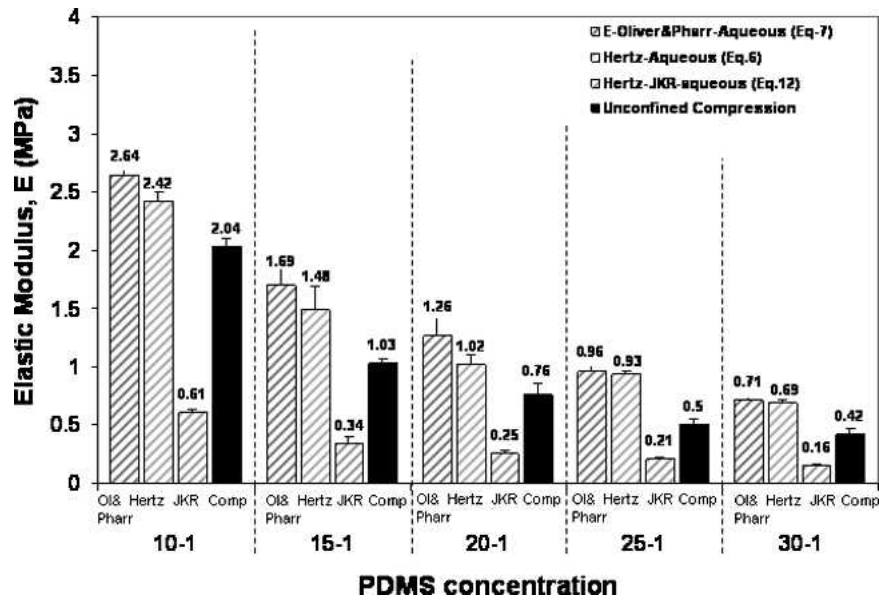


FIG. 9. Elastic moduli obtained from the nanoindentation experiments (aqueous conditions) using the Oliver and Pharr, Hertz, and JKR models (left to right). For comparison, the unconfined compression elastic moduli results are also shown for each PDMS concentration.

unconfined compression value. Following the analysis of Tabor,³¹ Muller et al.³⁹ showed that the two most common adhesion models (JKR and DMT) represent the extremes of a dimensionless parameter μ given by

$$\mu = \left(\frac{RW_A^2}{E_r^2 z_0^3} \right)^{1/3}, \quad (13)$$

where R is the tip curvature radius, and z_0 the equilibrium separation of the surfaces in the Lennard Jones potential ($z_0 = 2 \text{ \AA}$). It is shown that the magnitude of the pull-off force varies continuously from the DMT for $\mu < 0.1$ to the JKR value for $\mu > 5$. For the PDMS material in this study, using $W_A = 111 \text{ J/m}^2$ (calculated from an average pull-off force of $F_{po} \sim 70 \text{ \mu N}$), the average values for the elastic modulus ($\sim 1 \text{ MPa}$) and Poisson's ratio ($\nu_s = 0.5$) yield $\mu > 4000$. The aforementioned guideline suggests that the JKR model is appropriate for this application ($\mu > 5$). The discrepancy between bulk and JKR indentation data may then be rationalized by questioning the applicability of continuum ideal elastic mechanics models to soft substrates such as PDMS. Specifically, previous work⁴⁰ has shown some limitations in using nanoindentation for quantitatively determining material properties of soft and/or adhesive samples. There are uncertainties associated with the initial tip-sample contact point and tip shape at large depths. Such uncertainties may result in significant errors in calculating the absolute value of the elastic modulus. These limitations could explain the lower E_s values obtained when using JKR adhesive model. However, the qualitative behavior of the nanoindentation appears to be consistent with the unconfined compression measurements.

IV. CONCLUSIONS

Results from the unconfined compression and nanoindentation experiments indicate that there is a significant difference in the elastic modulus (E_s) of PDMS of different concentrations. Using the current protocol, the data indicate that nanoindentation is capable of measuring differences of hundreds of kilo-Pascals in elastic modulus. As expected, the elastic moduli decrease (2.04 to 0.42 MPa for unconfined compression) with increasing ratio of base to cross-linking agent, since increasing concentrations have more open (less cross-linking), flexible microstructures.

The PDMS elastic modulus values calculated from nanoindentation experiments using a Hertzian contact model are higher when compared to the unconfined compression results. These data indicate that the contact area is much larger than that estimated with the Hertzian model. Moreover, when testing is conducted in aqueous experiments, a significant decrease of the elastic modulus (compared to dry) is observed, though the values are still higher than unconfined compression measurements. This behavior seems to be related to a significant decrease in the work of adhesion due to the contribution of the electrostatic attraction. Adhesion models reconcile these differences. This suggests that the work of adhesion should not be ignored and plays a significant role in PDMS contact mechanics, even though absolute values from the JKR model calculations result in lower E_s . New developments in contact mechanics on a nanometer scale are necessary for a better understanding of these materials. Since soft material samples are expected to have significant adhesive forces, the work of adhesion must be included in the experimental protocol and evaluated

when determining mechanical properties with nanoindentation.

ACKNOWLEDGMENTS

The authors acknowledge financial support of the Department d'Universitats, Recerca i Societat de la Informació de la Generalitat de Catalunya, the Universitat Politècnica de Catalunya, the National Science Foundation and the National Institutes of Health/National Institute of Dental and Craniofacial Research Grant No. P01DE09859. The authors would like to thank Dr. Ravi Kiran Nalla from the Materials Science Division at E.O. Lawrence Berkeley National Laboratory for technical support with regard to the unconfined compression experiments.

REFERENCES

1. Y.C. Fung: *Biomechanics: Mechanical Properties of Living Tissues* (Springer-Verlag, New York, 1993).
2. W.C. Oliver and G.M. Pharr: An improved technique for determining hardness and elastic modulus using load and displacement sensing indentation experiments. *J. Mater. Res.* **7**, 1564 (1992).
3. W.C. Oliver and G.M. Pharr: Measurement of hardness and elastic modulus by instrumented indentation: advances in understanding and refinements to methodology. *J. Mater. Res.* **19**, 3 (2004).
4. J.Y. Rho, P. Zioupos, J.D. Currey, and G.M. Pharr: Variations in the individual thick lamellar properties within osteons by nanoindentation. *Bone* **25**, 295 (1999).
5. M.E. Roy, J.Y. Rho, T.Y. Tsui, N.D. Evans, and G.M. Pharr: Mechanical and morphological variation of the human lumbar vertebral cortical and trabecular bone. *J. Biomed. Mater. Res.* **44**, 191 (1999).
6. P.K. Zysset, X.E. Guo, C.E. Hoffler, K.E. Morre, and S.A. Goldstein: Elastic modulus and hardness of cortical and trabecular bone lamellae measured by nanoindentation in the human femur. *J. Biomech.* **32**, 1005 (1999).
7. X.E. Guo and S.A. Goldstein: Vertebral trabecular cone microscopic tissue elastic modulus and hardness do not change in ovariectomized rates. *J. Orthop. Res.* **18**, 333 (2000).
8. L. Guo, X. Guo, Y. Leng, J.C. Cheng, and X. Zhang: Nanoindentation study of interfaces between calcium phosphate and bone in an animal spinal fusion model. *J. Biomed. Mater. Res.* **54**, 554 (2001).
9. J.Y. Rho, J.D. Currey, P. Zioupos, and G.M. Pharr: The anisotropic Young's modulus of equine secondary osteons and interstitial bone determined by nanoindentation. *J. Exp. Biol.* **204**, 1775 (2001).
10. J.G. Swadener, J.Y. Rho, and G.M. Pharr: Effects of anisotropy on elastic moduli measured by nanoindentation in human tibial cortical bone. *J. Biomed. Mater. Res.* **57**, 108 (2001).
11. S. Hengsbarger, A. Kulik, and P. Zysset: Nanoindentation discriminates the elastic properties of individual human bone lamellae under dry and physiological conditions. *Bone* **30**, 178 (2002).
12. G.W. Marshall, S. Habelitz, R. Gallagher, M. Balooch, G. Balooch, and S.J. Marshall: Nanomechanical properties of hydrated carious human dentin. *J. Dent. Res.* **80**, 1768 (2000).
13. M. Balooch, I.C. Wumagidi, A. Balazs, A.S. Lundkvist, S.J. Marshall, G.W. Marshall, W.J. Siekhaus, and J.H. Kinney: Viscoelastic properties of demineralized human dentin measured in water with atomic force microscope (AFM)-based indentation. *J. Biomed. Mater. Res.* **40**, 539 (1998).
14. D.M. Ebenstein, A. Kuo, J.J. Rodrigo, A.H. Reddi, M. Ries, and L.A. Pruitt: Nanoindentation technique for functional evaluation of cartilage repair tissue. *J. Mater. Res.* **19**, 273 (2004).
15. D.M. Ebenstein and L.A. Pruitt: Nanoindentation of soft hydrated materials for application to vascular tissues. *J. Biomed. Mater. Res. A* **69A**, 222 (2004).
16. S. Gupta, F. Carrillo, M. Balooch, L. Pruitt, and C.M. Puttlitz: Simulated soft tissue nanoindentation—A finite element study. *J. Mater. Res.* **20**, 1979 (2005).
17. D. Maugis: *Contact, Adhesion and Rupture of Elastic Solids* (Springer, New York, 1999).
18. K.R. Shull, D. Ahn, W.L. Chen, C.M. Flanagan, and A.J. Crosby: Axisymmetric adhesion tests of soft materials. *Macromol. Chem. Phys.* **199**, 489 (1998).
19. S.J. Clarson and J.A. Semlyen: *Siloxane Polymers* (Prentice-Hall, Englewood Cliffs, NJ, 1993).
20. C. Livermore and J. Voldman: Material properties database. <http://www.mit.edu/~6.777/matprops/matprops.htm> (2005).
21. C.C. White, P.L. Drzal, and M.R. VanLandingham: Viscoelastic characterization of polymers using dynamic instrumented indentation, in *Fundamentals of Nanoindentation and Nanotribology III*, edited by K.J. Wahl, N. Huber, A.B. Mann, D.F. Bahr, and Y-T. Cheng (Mater. Res. Soc. Symp. Proc. **841**, Warrendale, PA, 2005), R5.3 p. 187.
22. J.C. Lötters, W. Olthuis, P.H. Veltink, and P. Bergveld: Polydimethylsiloxane as an elastic material applied in a capacitive accelerometer. *J. Micromech. Microeng.* **6**, 52 (1996).
23. J.C. Lötters, W. Olthuis, P.H. Veltink, and P. Bergveld: The mechanical properties of the rubber elastic polymer polydimethylsiloxane for sensor applications. *J. Micromech. Microeng.* **7**, 145 (1997).
24. K.G. Sharp, G.S. Blackman, N.J. Glassmaker, A. Jagota, and C.Y. Hui: Effect of stamp deformation on the quality of micro-contact printing: Theory and experiment. *Langmuir* **20**, 6430 (2004).
25. D.L. Sedin and K.L. Rowlen: Influence of tip size on AFM roughness measurements. *Appl. Surf. Sci.* **182**, 40 (2001).
26. H. Hertz: On the contact of elastic solids. *J. Reine Angew. Math.* **92**, 156 (1881).
27. K.L. Johnson: *Contact Mechanics* (Cambridge University Press, Cambridge, U.K., 1987).
28. I.N. Sneddon: The relation between load and penetration in the axisymmetric Boussinesq problem for a punch of arbitrary profile. *Int. J. Eng. Sci.* **3**, 47 (1956).
29. K.L. Johnson, K. Kendall, and A.D. Roberts: Surface energy and the contact of elastic solids. *Proc. R. Soc. London* **A324**, 301 (1971).
30. B.V. Derjaguin, V.M. Muller, and Y.P. Toporov: Effect of contact deformations on the adhesion of particles. *J. Colloid Interface Sci.* **53**, 314 (1975).
31. D. Tabor: Surface forces and surface interactions. *J. Colloid Interface Sci.* **58**, 2 (1977).
32. D. Maugis: Adhesion of spheres: the JKR-DMT transition using a Dugdale model. *J. Colloid Interface Sci.* **150**, 243 (1992).
33. K.L. Johnson and J.A. Greenwood: An adhesion map for the contact of elastic spheres. *J. Colloid Interface Sci.* **192**, 326 (1997).

34. R.W. Carpick, D.F. Ogletree, and M. Salmeron: A general equation for fitting contact area and friction vs load measurements. *J. Colloid Interface Sci.* **211**, 395 (1999).
35. Y.J. Sun, B. Akhremitchev, and G.C. Walker: Using the adhesive interaction between atomic force microscopy tips and polymer surfaces to measure the elastic modulus of compliant samples. *Langmuir* **20**, 5837 (2004).
36. A. Galliano, S. Bistac, and J. Schultz: Adhesion and friction of PDMS networks: Molecular weight effects. *J. Colloid Interface Sci.* **265**, 372 (2003).
37. A. N. Gent and J. Schultz: Effect of wetting liquids on the strength of adhesion of viscoelastic materials. *J. Adhes.* 281 (1972).
38. N.S. Tambe and B. Bhushan: Scale dependence of micro/nano-friction and adhesion of MEMS/NEMS materials, coatings and lubricants. *Nanotechnology* **15**, 1561 (2004).
39. V.M. Muller, V.S. Yushman, and B.V. Derjaguin: On the influence of molecular forces on the deformation of an elastic sphere and its sticking to a rigid plane. *J. Colloid Interface Sci.* **77**, 91 (1980).
40. M.R. VanLandingham, P.L. Drzal, and C.C. White: Indentation creep and relaxation measurement of polymers, in *Fundamentals of Nanoindentation and Nanotribology III*, edited by K.J. Wahl, N. Huber, A.B. Mann, D.F. Bahr, and Y-T. Cheng (Mater. Res. Soc. Symp. Proc. **841**, Warrendale, PA, 2005), R5.5, p. 193.